

## Efficient coagulation and removal of aqueous graphene oxide by different dyes

Xiaobin Zhu<sup>a,\*</sup>, Jinlei Zhang<sup>b</sup>, Shuyi Wu<sup>b</sup>, Zhengcun Zhou<sup>a</sup>

<sup>a</sup>School of Mechano-Electronic Engineering, Suzhou Vocational University, Suzhou, Jiangsu 215104, China, emails: zxbblack@163.com (X.B. Zhu), zzc@jssvc.edu.cn (Z.C. Zhou)

<sup>b</sup>Jiangsu Key Laboratory of Micro and Nano Heat Fluid Flow Technology and Energy Application, School of Mathematics and Physics, Suzhou University of Science and Technology, Suzhou, Jiangsu 215009, China, emails: zhangjinlei199119@126.com (J.L. Zhang) woaiwuliban@163.com (S.Y. Wu)

Received 27 February 2020; Accepted 1 December 2020

---

### ABSTRACT

Despite graphene oxide (GO)'s excellent physical and chemical properties, recent researches suggest its toxicity in biological applications. In this study, three dyes, methylene blue (MB), rhodamine-B (RhB) and methyl orange (MO), are used as coagulants to remove GO from aqueous solution. Results show that MB has the best performance with maximum coagulation capacity up to 2.27 g/g, higher than that of most other coagulants. Electrostatic interaction plays a key role in coagulation, also aided by  $\pi$ - $\pi$  stacking interaction. Besides its great coagulation capacity, MB itself is a pollutant abundant in many types of wastewater, providing a readily accessible reagent, which makes it more suitable for the application.

*Keywords:* Coagulation; Graphene oxide; Methylene blue; Electrostatic interaction

---

### 1. Introduction

Graphene gains rapid popularity in recent years [1,2]. As opposed to ideal graphene, soluble graphene oxide (GO), is more commonly adopted due to its accessibility [3–8]. So far, GO demonstrates great advantages in many fields as energy [3,4], environment governing [5,6] and biomedical applications [7,8]. Meanwhile, some researchers point out that GO, like other graphene related materials, may be toxicity and many experiments have shown that GO has toxic side effects in biological applications [9,10]. An influx of soluble GO into the aquatic ecosystem will be inevitable once large scale application of GO becomes a reality. This demands an efficient way to treat waste GO solution.

Up to now, several methods such as photo-induced degradation [11,12] and coagulation [13–19] have been used to remove GO. Yuan et al. [11] reported that GO can be completely degraded within 12 h at pH = 5 under 500 W high-pressure Mercury lamp with maximum wavelength at

365 nm. The degradation time is up to 3 d when using the photo-Fenton method [12]. Thus these two methods suffer the obvious shortcoming of extended reaction time.

Contrarily, the coagulation process is faster than many other separation techniques such as evaporation, membrane separation and photo-induced degradation. Since coagulation is easy to operate and consumes no extra energy, it is more suitable for the application. Aluminum-based materials are the commonly used coagulants [13–16,18]. Wang et al. [14] reported Mg/Al and Ca/Al layered double hydroxides (LDHs) exhibited maximum GO removal capacities of 79.9 and 123 mg/g. The removal capacities will increase significantly after the LDHs are calcined. Yuan et al. [18] found that MgAl-mixed metal oxide (MgAl-MMO) synthesized by one-step calcination of MgAl-LDH showed a much better removal capacity of 984.2 mg/g. The mechanism of GO removal using MgAl-MMO composite was the memory effect. Alum is also a good coagulant whose removal capacity is 960 mg/g [17]. Alum is different from

---

\* Corresponding author.

the coagulants mentioned above as it is soluble, which means that soluble materials can also be used as coagulants. The study of coagulants other than aluminum-based materials is few. Recently, Yuan et al. [19] found that cement can act as a coagulant, which owns the highest removal capacity of 5,981.2 mg/g up to now. As far as we know, it is the only coagulant whose removal capacity exceeds 1,000 mg/g. Yuan et al. [19] believed that one of the mechanisms of GO removal by cement was  $\text{Ca}^{2+}$ -induced coagulation.

The coagulants mentioned above share a common drawback: they introduce ions into the water which requires further treatment. This drawback naturally disappeared if we choose dyes as coagulants. This is possible because they can be adsorbed onto GO in aqueous solution due to electrostatic interaction and  $\pi$ - $\pi$  stacking interaction [6,20–25]. Meanwhile, dyes degrade much more easily. The time required is less than 80 min as opposed to 3 d for that of GO by Fenton reaction [12,22]. In addition, dyes are present in many types of wastewater, which serves as a reagent free of charge. Thus dyes seem to be promising candidates for our purpose. In this study, three dyes, methylene blue (MB), rhodamine-B (RhB) and methyl orange (MO), are investigated. The initial concentrations of GO and dyes are varied to find the best ratio of dye to GO. The coagulation mechanism has also been discussed, with the electrostatic interaction being the major contributor of coagulation.

## 2. Experimental section

### 2.1. Materials

The GO sheet (ID XF002-1) was purchased from Jiangsu XFANO Materials Tech. Co., Ltd. (Nanjing, China) and the other chemicals including activated charcoal powder (ACP), MB (indicator grade), MO (indicator grade) and RhB were obtained from Sinopharm Chemical Reagent Co., Ltd. (China). MB and MO were of indicator grades and the other chemicals were of analytical grade. All the chemicals were used as received without further purification. Deionized (DI) water was used in all the experiments.

### 2.2. Preparation of GO suspension

The pristine GO suspension was prepared by an ultrasonic method.  $x$  mg GO sheet was added to a beaker containing 80 mL DI water and then the mixture was ultrasonically treated. To prevent GO from degradation by heating, the ultrasonic treatment was shut down every 30 min and restarted 30 min later. After being treated for 12 h, the suspension was diluted to 100 mL. The concentration of GO suspension can be expressed as  $C_{\text{GO}} = 10 \cdot x$  mg/L. The centrifuged GO suspension was prepared by centrifuging the pristine GO suspension three times at 6,000 rpm for 5 min.

### 2.3. Coagulation experiments

All the ultraviolet-visible (UV-Vis) absorption spectra were obtained using a double beam UV/VIS spectrophotometer (Rayleigh UV-2601, China). When the concentration of the suspension is too high, the suspension was diluted  $n$  ( $n = 2, 4, 5$  or  $8$ ) times before measured by UV-Vis

spectrophotometer. The measured spectrum was multiplied by  $n$  and the obtained spectrum was regarded as the absorption spectrum of the suspension. The concentration of GO was determined by the UV-Vis absorption spectra at the wavelength of 228 nm. The initial concentration was calculated by dividing mass by total volume of GO suspension and dye solution (10 mL) if there was no special explanation.

In the preliminary coagulation experiments, 5 mL pristine GO suspension was added to 5 mL MB solution with different concentrations. After the mixture was stirred for an hour and rested for another hour, the supernatant suspension was monitored by UV-Vis spectrometer. In the modified coagulation experiments, 5 mL of the centrifuged GO suspension was added to 5 mL dye solution with different concentrations. After the mixture was stirred for an hour and rested for another hour, adequate ACP (40 times the mass of initial MB) was added to the mixture. The suspension is stirred for an hour and rested for another hour. Finally, the supernatant suspension was centrifuged at 6,000 rpm for 5 min to remove the precipitate and the suspension was monitored by UV-Vis spectrometer.

As the equilibrium concentration ( $C_e$ ) was recorded after centrifugation, the measured concentration would be a little lower than the actual value. To eliminate the influence of centrifugation, a reference GO suspension with the same initial concentration as the suspension for coagulation experiments were centrifuged at 6,000 rpm for 5 min and the concentration of the supernatant suspension was used as the initial concentration ( $C_0$ ). The coagulation capacity ( $q_e$ ) and the removal percentage ( $R$ ) for GO were calculated using the following equations:

$$q_e = \frac{C_0 - C_e}{C_{\text{dye}}} \quad (1)$$

$$R = \frac{C_0 - C_e}{C_0} \times 100\% \quad (2)$$

where  $C_{\text{dye}}$  was the initial concentration of dye.

## 3. Results and discussion

The concentration of GO suspension was linearly related to its absorbance at the maximum absorption wavelength [11,13–19]. However, the peak positions as well as the absorption coefficient ( $\alpha$ ) were different in different works [11,13–19]. This was mainly caused by variance of sizes and oxidation degrees of GO. So we studied the correlation between the concentration of GO suspension and absorbance before coagulation experiments. As presented in Fig. S1a, the absorption peaks of GO suspension all appeared at the wavelength of 228 nm. The concentration of GO suspension is linearly related to the absorbance at 228 nm provided GO concentration is no more than 50 mg/L (Fig. S1b), with an absorption coefficient of 37.08 L/(g cm).

Fig. 1 shows the absorption spectra and the photographs of the GO suspension after coagulation in the preliminary coagulation experiments. The initial GO concentration was maintained at 50 mg/L and the initial MB concentration was varied at 2, 10 and 50 mg/L, respectively. When the

initial MB concentration was low (2 or 10 mg/L), coagulations could not be observed in the photographs (Figs. 1b and c). The absorbance at 228 nm increased with the addition of low concentration MB, giving no evidence of coagulation. When the initial MB concentration increased to 50 mg/L, precipitate occurred (Fig. 1d). Meanwhile, the absorbance at 228 nm decreased and the ratio of absorbance at different wavelengths matched that of the absorption spectrum of 5 mg/L MB solution (Fig. S2a), which indicated removal of most GO by coagulation. The absorbance at the maximum absorption wavelength of MB (664 nm) of the coagulated suspension was 5.615 and the concentration was calculated to be 24.8 mg/L. This means approximately half of the MB participated in the coagulation.

The accurate amount of residual GO was difficult to work out due to the effect of MB on absorption, hence was the coagulation capacity. An adsorbent for MB, which did not interact with GO was needed to eliminate the influence of the dissolved MB. Several adsorbents were tested and the ACP turned out to be the optimum selection. Different amounts of ACP (50–400 mg/L) were added to MB aqueous solution (5 mg/L), and ACP was separated by centrifugation

(6,000 rpm; 5 min) after adequate adsorption. Fig. S3 shows the UV-Vis spectra of MB aqueous solutions after adsorption. When the amount of adsorbent was higher than 200 mg/L (40 times the mass of MB), the absorption peak at 664 nm disappeared completely confirming the absence of MB. Fig. S4 shows the effect of centrifugal times on GO concentration. After initial centrifugation, 1.51% GO was removed. The subsequent centrifugations had little effect on the GO concentration, removing a mere 0.32% of GO after three centrifugations. The centrifuged GO suspension, which had been prepared by centrifuging the pristine GO suspension three times at 6,000 rpm for 5 min was used in the subsequent experiments to reduce the influence of centrifugation on GO concentration. The interaction of the centrifuged GO and ACP was also investigated, and the absorbance as well as the removal percentage of GO suspension after adsorption in the presence of ACP is shown in Fig. S5. Despite the amount of ACP was as high as 160 mg (320 times of that of GO), only 1.2% GO was removed. These results put ACP an ideal adsorbent to remove extra MB and to reveal the presence of residual GO after coagulation.

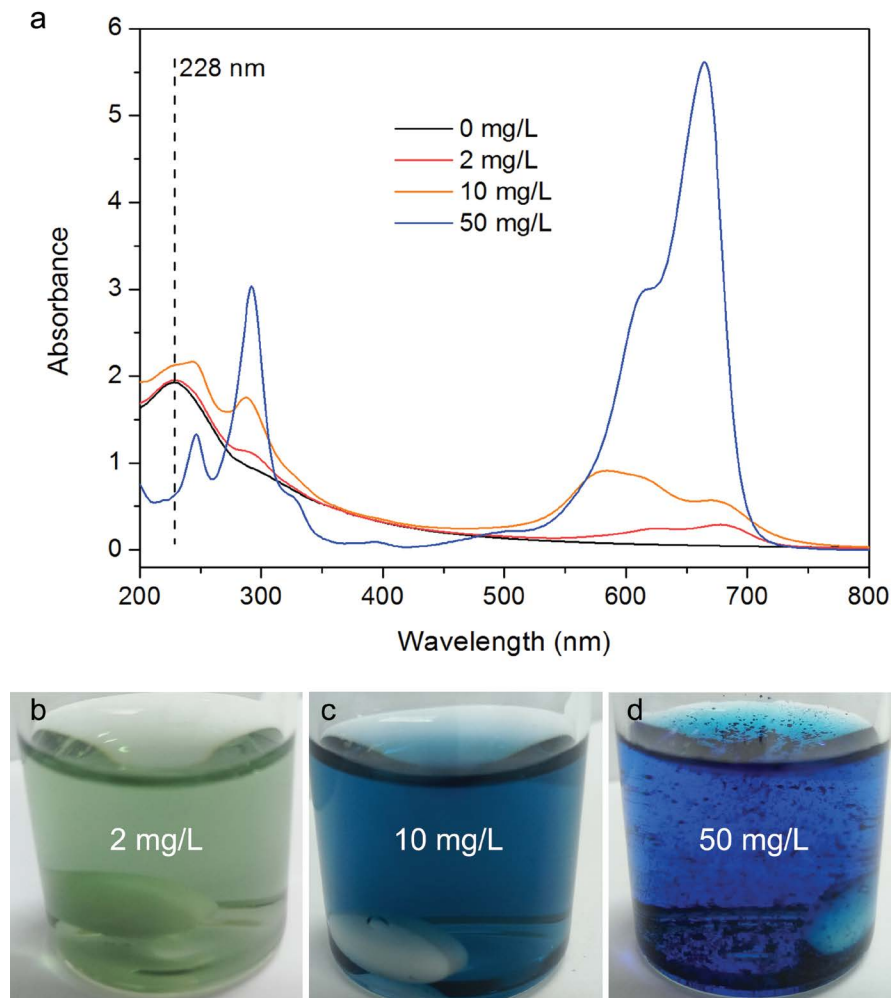


Fig. 1. (a) Absorption spectra and (b–d) digital photographs of the GO suspension after coagulation in the preliminary coagulation experiments.

The modified coagulation experiments were carried out by replacing the pristine GO suspension with the centrifuged GO suspension, and adequate ACP (40 times the mass of initial MB) was used subsequently to remove dissolved MB. Figs. 2a–d show the digital photographs before ACP was added. When the initial MB concentration was low (6.25 or 12.5 mg/L), coagulation was not obvious (Figs. 2b and c). Coagulation became apparent when the concentration reached 25 mg/L (Fig. 2d) and substantial MB was removed in this process (Fig. 2a). This is consistent with the results of our preliminary experiments. After ACP was added and the suspension was centrifuged, the final suspension became clear when the initial MB concentration was higher than 25 mg/L (Figs. 2e and f). The color of the final suspension was yellow-green, which was different from the reference GO suspension when the initial MB concentration was lower than 12.5 mg/L.

The UV-Vis absorption spectra of the final suspension are shown in Fig. 3a. When the initial MB concentration

was 6.25 mg/L, the absorbance at 228 nm was almost the same as the reference sample. The absorbance at 295, 633 and 675 nm of the tested sample was higher than that of the reference sample, and small shoulder peaks could be seen at these wavelengths. This was consistent with the optical pictures in Fig. 2f. The position of shoulder peaks was close to that of MB absorption peaks at 292, 616 and 664 nm (Fig. S2a) [20]. So it could be speculated that the shoulder peaks were formed due to the absorbance of MB. Our earlier experiment had shown that the dissolved MB could be completely removed when the added ACP was more than 40 times the mass of MB. We could infer that the residual MB in the modified coagulation experiment was not dispersed in water but adsorbed by GO to form a composite [25]. The interaction between MB and GO in the composite was stronger than that between MB and ACP. The adsorbed MB concentration could be calculated to be 0.425 mg/L, which was about 6.8% of the initial concentration by the difference of absorbance at 228 nm. When the

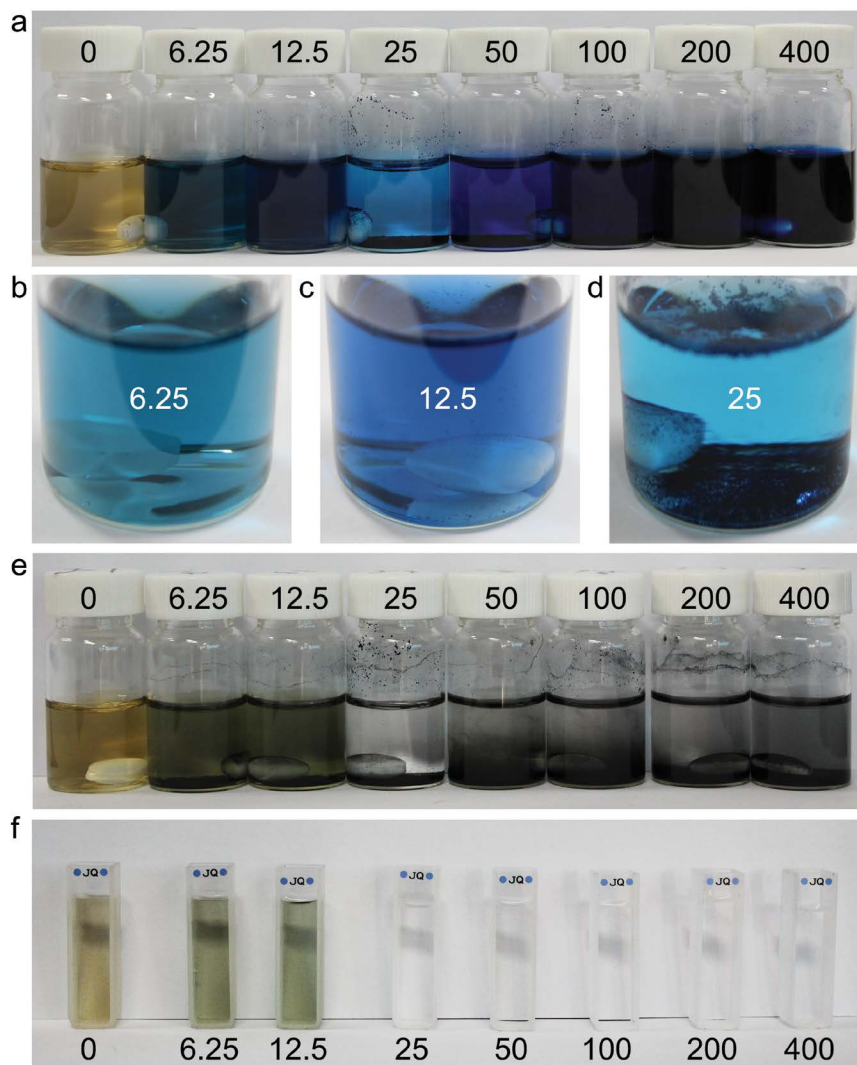


Fig. 2. Digital photographs in the modified coagulation experiments (a–d) before and (e) after ACP was added. (f) Digital photographs taken after the suspension was centrifuged. The labeled number represents the initial MB concentration.

initial MB concentration was 12.5 mg/L, the absorbance at 228 nm decreased slightly (Fig. 3M), indicating that a small amount of GO had been removed. The shoulder peaks also appeared, and the intensities of these peaks did not change much. When the initial MB concentration reached 25 mg/L, the absorbance at 228 nm decreased rapidly. The removal rate increased from 4.6% to 93.7% (Fig. 3c). When the initial MB concentration was higher than 50 mg/L, most of the GO was removed. The GO coagulation capacities were displayed in Fig. 3d. With the increase of initial MB concentration, the coagulation ability first increased and then decreased. The coagulation capacity reached the maximum value of 1.89 g/g at an initial MB concentration of 25 mg/L.

The initial GO concentration may also affect coagulation. So coagulation experiments with different initial GO concentration (25, 100, 200 and 400 mg/L) was carried out, and the absorption spectra were shown in Fig. S6. The absorption spectra in each group had the same features. First, the absorbance at 228 nm decreased with the increase

of MB concentration. Second, the shoulder peak due to the adsorbed MB appeared at low MB concentration. These two features were the same as those of experiments with an initial concentration of 50 mg/L. Fig. 3e shows the removal rate after the coagulation experiments with different initial GO concentration. When the initial GO concentrations were 25, 50 and 100 mg/L, the scatter plots almost coincided with each other. The removal rate changed suddenly as the initial concentration ratio of MB and GO ( $C_{MB}/C_{GO}$ ) increased from 1/4 to 1/2, and most GO (more than 90%) will be removed when the initial MB concentration reached 25 mg/L. When the initial GO concentration increased to more than 200 mg/L, the removal rate at a small initial concentration ratio (1/8 and 1/4) became larger, while the removal rate at a large initial concentration ratio (larger than 1/2) became smaller. The coagulation capacity all reached the maximum value at an initial concentration ratio of 1/2 for different initial GO concentration (25 to 400 mg/L), and the maximum coagulation capacities were 1.89, 1.89, 1.87, 1.59 and 0.74 g/g

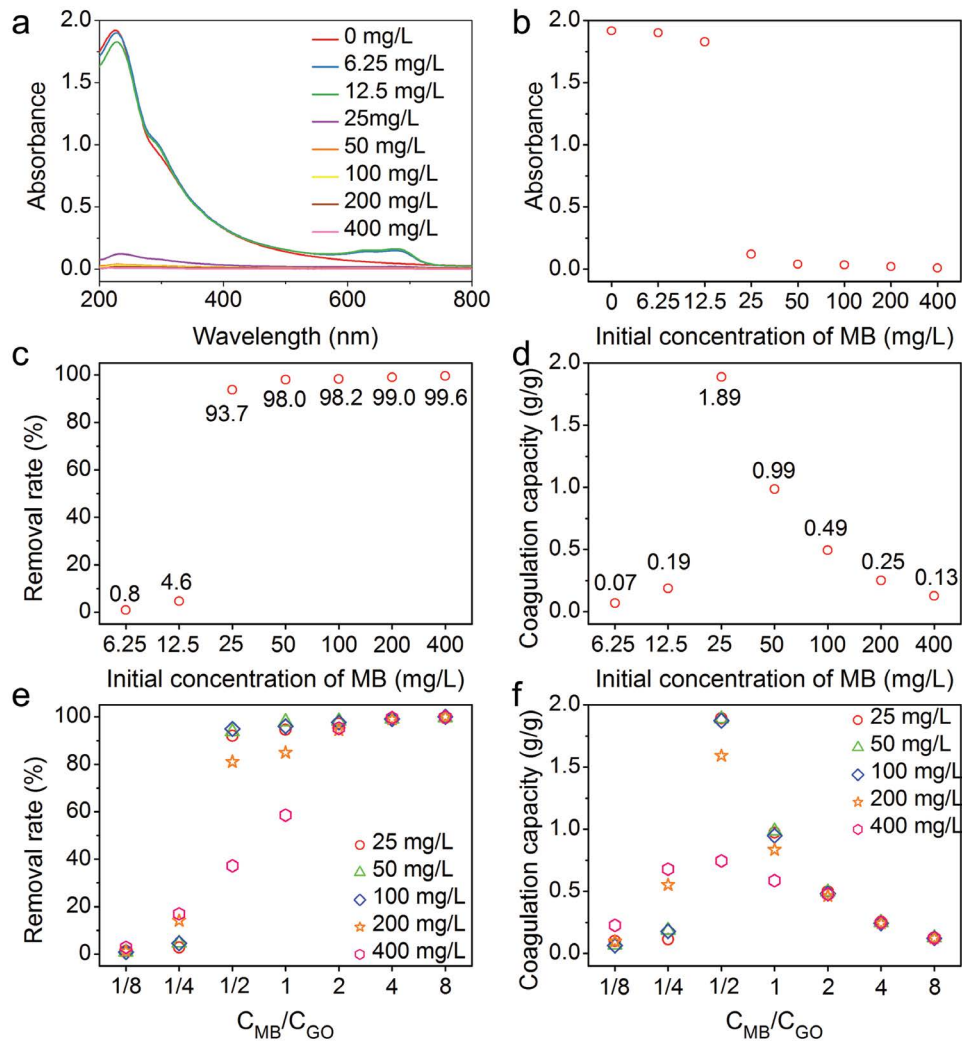


Fig. 3. (a) Absorption spectra, (b) absorbance at 228 nm, (c) removal rates and (d) coagulation capacities after the modified coagulation experiments when the initial GO concentration was 50 mg/L. (e) Removal rates and (f) coagulation capacities after the modified coagulation experiments with different initial GO concentration (25–400 mg/L). The initial concentration ratio of MB and GO ranged from 1/8 to 8.

(Fig. 3f). MB poses a better coagulation capacity with GO when the initial GO concentration is no more than 100 mg/L.

The sudden change in removal rate as  $C_{MB}/C_{GO}$  increased from 1/4 to 1/2 was noteworthy. This demands a more detailed experimental study within this range. Since the coagulation behavior was similar at different initial GO concentrations, we only studied the case in which the initial GO concentration was 50 mg/L. Fig. 4a shows the absorption spectra with initial MB concentration increasing from 12.5 to 25 mg/L. The absorption peak of GO and MB decreased as initial MB concentration increased. The adsorption capacities of MB on the uncoagulated GO estimated by absorbance at 228 and 664 nm were less than 30 mg/g (Fig. 4b), which is far less than the maximum adsorption capacity of 714 mg/g [25]. The removal rates of GO increased as initial MB concentration increased (Fig. 4c). Most GO (90.1%) was removed and the coagulation capacity reached the maximum value of 2.27 g/g at initial MB concentration of 20 mg/L (Fig. 4d). The coagulation capacities of several coagulants proposed by others are listed in Table 1 [13–19]. In comparison, MB excels in its coagulation capacity, only second to cement. An additional advantage is that, MB itself is a contaminant that needs to be treated. No additional cost is incurred when MB and GO are treated together. More importantly, GO takes away part of MB during coagulation, which in turn reduces the cost of MB treatment. In sum MB possess the unique advantage of introducing benefits instead of expenditure.

The coagulation capacities for GO in the presence of other dyes had been also studied. We chose anionic dye (MO) and a cationic dye (RhB) as the coagulants. Fig. 5a shows the absorption spectra of GO in MO aqueous

suspensions. Unlike in MB aqueous suspension, absorbance did not decrease but increased even though the initial MO concentration reached 400 mg/L. The maximum absorbance increment appeared at 228 nm which was also the maximum absorbance position of MO (Fig. S2b). So the enhancement of absorbance could be attributed to the adsorption of MO by GO. Figs. 5b–d show the absorption spectra, digital photographs and the removal rates of GO in RhB aqueous suspensions. When the concentration of RhB did not exceed 50 mg/L, absorbance at 228 nm changed little, and no obvious precipitates were observed in the digital photographs. Shoulder peaks appeared near 565 nm, which corresponded to the absorption peak of

Table 1  
Comparisons of the coagulation capacity of GO with different coagulants

Coagulants	Removal capacity (mg/g)	References
Mg/Al LDH-Cl	57	13
Mg/Al LDH	79.9	14
Ca/Al LDH	123	14
LDO-GI	448.3	15
Ca/Al/La-CLDHs	558.6	16
Mg/Al/La-CLDHs	565.8	16
Alum	960	17
MgAl-MMO	984.2	18
Cement	5,981.2	19
MB	2,268	This study

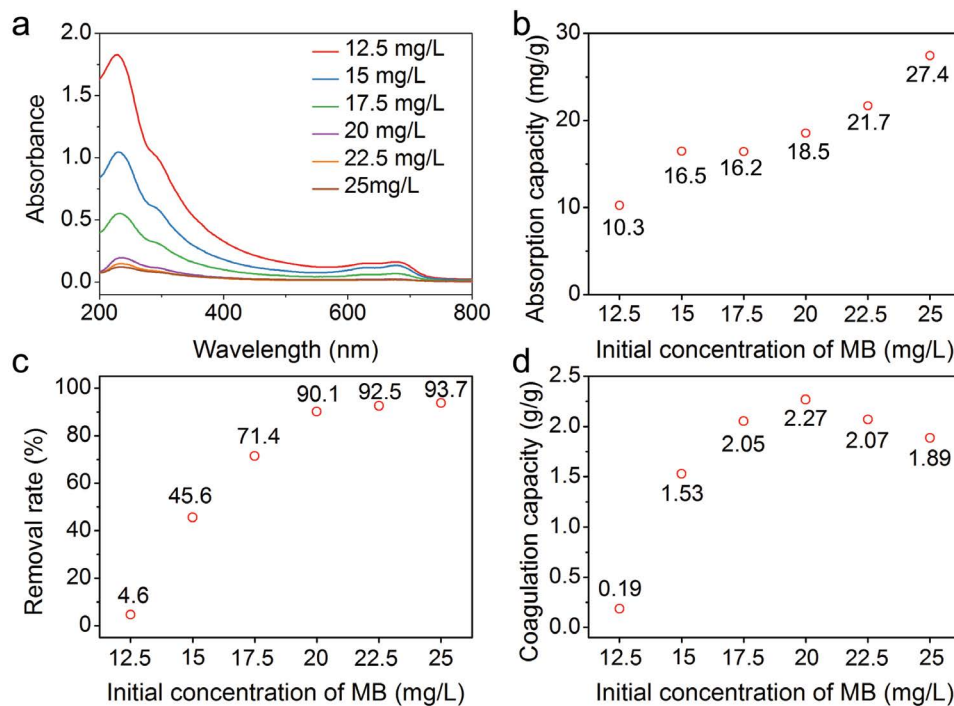


Fig. 4. (a) Absorption spectra, (b) adsorption capacity of MB on the uncoagulated GO, (c) removal rates and (d) coagulation capacities with initial MB concentration increasing from 12.5 to 25 mg/L.

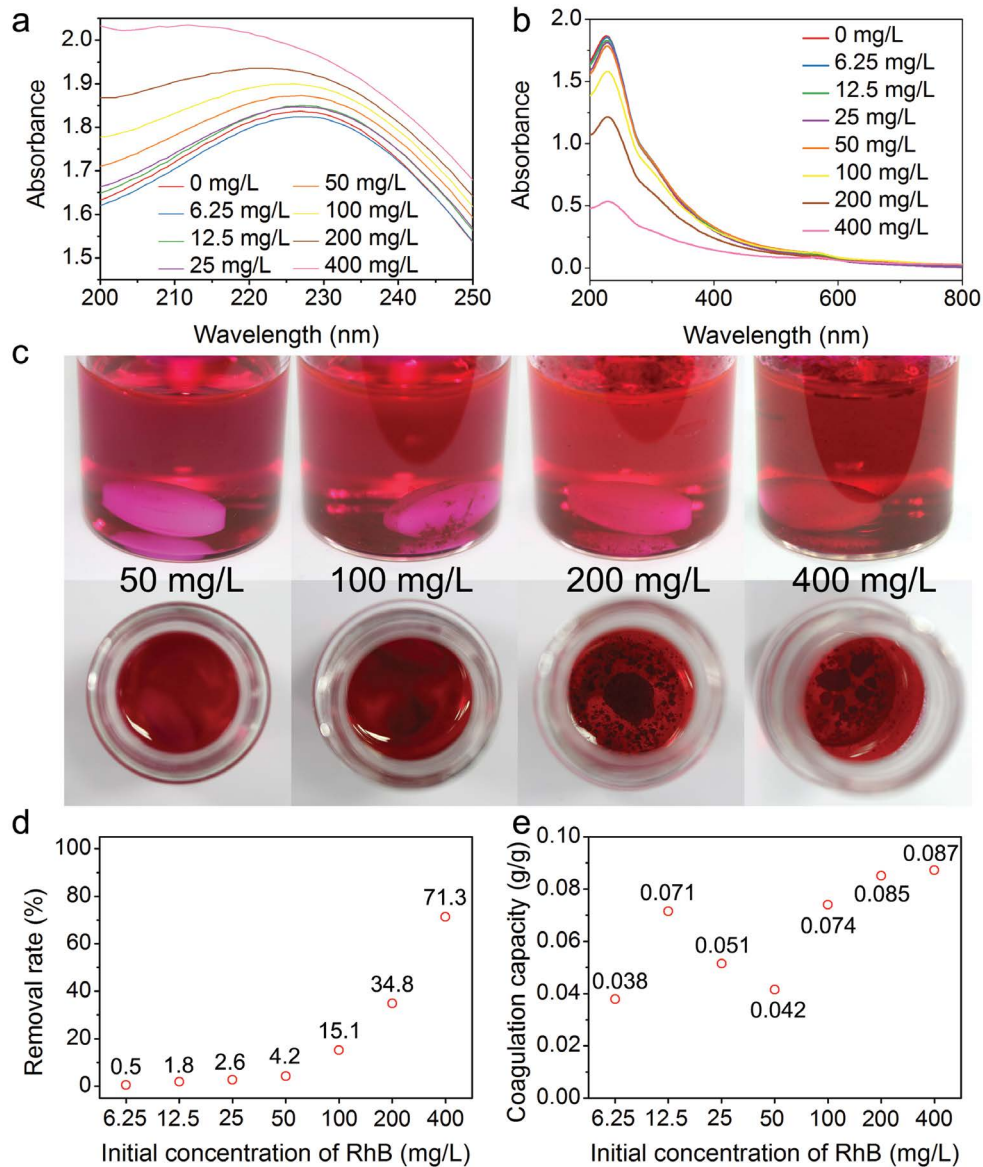


Fig. 5. (a) Absorption spectra of GO in MO aqueous suspensions. (b) The absorption spectra (c) digital photographs (d) removal rates and (e) coagulation capacities of GO in RhB aqueous suspensions.

RhB (Fig. 2c). Precipitates appeared as RhB concentration reached 100 mg/L. Subsequently, the removal rate of GO increased evidently with the increase of RhB concentration, reaching a maximum removal rate of 71.3%. The maximum coagulation capacity of RhB was 0.087 mg/g, far less than that of MB.

Up to now, various mechanisms were used to illustrate the aggregation of GO by coagulants, including electrostatic interactions, hydrogen bonds, bridging function, surface complexation and memory effect [13–19]. Regardless of the coagulation mechanism, coagulation occurs only when coagulants interact with GO to form a composite. It is well known that cationic dyes can be adsorbed onto GO due to electrostatic interaction and  $\pi$ - $\pi$  stacking interaction, and electrostatic interaction plays the major role. The maximum adsorption capacity of GO for MB and

RhB are 714 and 201 mg/g [25,26]. Therefore, adsorption occurred between the GO and cationic dyes, at the early stage of coagulation. This adsorption neutralized part of the charge and reduced the electrostatic repulsion, so GO tended to agglomerate and precipitate eventually. It can be further inferred that the stronger the adsorption ability of GO to dyes, the greater the coagulation. This is consistent with our coagulation experiments. It is noteworthy experimentally that when the initial GO concentration is more than 200 mg/g, the maximum coagulation capacity of MB decreases (Fig. 3f). As the coagulation capacity all reached the maximum value at the initial concentration ratio of 1/2, the initial MB concentration will be higher when the initial GO concentration is higher. At this time, MB monomers tend to convert into dimers [27]. There will be interaction between the two monomers of

the dimer, weakening the interaction between MB and GO, which consequently reduces the coagulation ability. GO and MO are both anionic, and the maximum adsorption capacity of GO for MO is only 16.83 mg/g [24,28]. So GO does not coagulate with MO. To sum up, the major contributor of coagulation is the electrostatic interaction, while the  $\pi$ - $\pi$  stacking only plays a minor role.

#### 4. Conclusion

As a cationic dye, MB is a good GO coagulant with excellent performance when GO concentration is no more than 100 mg/L. The maximum coagulation capacity measured reaches 2.27 g/g, higher than that of most other coagulants. RhB can also be used as a coagulant, with lower coagulation capacity. Contrarily, the coagulation of GO was not observed in the presence of MO. Electrostatic interaction serves as the main driver of coagulation, while the  $\pi$ - $\pi$  stacking interaction contributes slightly to the whole interaction. MB is a pollutant that needs to be removed from sewage. No additional cost is incurred to remove GO when MB and GO are treated together. Meanwhile, GO takes away part of MB during coagulation, which in turn reduces the cost of MB treatment. Therefore, MB is not only an efficient coagulant but also an economical coagulant, making it an ideal candidate for the application.

#### Acknowledgments

This work was supported by Natural Science Foundation of Jiangsu Province (BK20171225), Livelihood Project of Suzhou Municipal Science and Technology Bureau (SS201817) and Research Foundation of Suzhou Vocational University (SVU2018YY08). Partial support was also from Natural Science Foundation of the Jiangsu Higher Education Institutions of China (19KJD470005).

#### References

- [1] A.K. Geim, K.S. Novoselov, The rise of graphene, *Nat. Mater.*, 6 (2007) 183–191.
- [2] C.L. Tan, X.H. Cao, X.J. Wu, Q.Y. He, J. Yang, X. Zhang, J.Z. Chen, W. Zhao, S.K. Han, G.H. Nam, M. Sindoro, H. Zhang, Recent advances in ultrathin two-dimensional nanomaterials, *Chem. Rev.*, 117 (2017) 6225–6331.
- [3] H.J. Yan, Y. Xie, Y.Q. Jiao, A.P. Wu, C.G. Tian, X.M. Zhang, L. Wang, H.G. Fu, Holey reduced graphene oxide coupled with an Mo<sub>2</sub>N-Mo<sub>2</sub>C heterojunction for efficient hydrogen evolution, *Adv. Mater.*, 30 (2018) 1704156.
- [4] Y.Q. Wu, P. Wang, X.L. Zhu, Q.Q. Zhang, Z.Y. Wang, Y.Y. Liu, G.Z. Zou, Y. Dai, M.H. Whangbo, B.B. Huang, Composite of CH<sub>3</sub>NH<sub>2</sub>PbI<sub>3</sub> with reduced graphene oxide as a highly efficient and stable visible-light photocatalyst for hydrogen evolution in aqueous HI solution, *Adv. Mater.*, 30 (2018) 1704342.
- [5] D.F. Xu, B. Cheng, W.K. Wang, C.J. Jiang, J.G. Yu, Ag<sub>2</sub>CrO<sub>4</sub>/G-C<sub>3</sub>N<sub>4</sub>/graphene oxide ternary nanocomposite Z-scheme photocatalyst with enhanced CO<sub>2</sub> reduction activity, *Appl. Catal. B*, 231 (2018) 368–380.
- [6] X.B. Zhu, Y. Shan, S.J. Xiong, J.C. Shen, X.L. Wu, Brianyoungite/graphene oxide coordination composites for high-performance Cu<sup>2+</sup> adsorption and tunable deep-red photoluminescence, *ACS Appl. Mater. Interfaces*, 8 (2016) 15848–15854.
- [7] B. Han, Y.L. Zhang, L. Zhu, Y. Li, Z.C. Ma, Y.Q. Liu, X.L. Zhang, X.W. Cao, Q.D. Chen, C.W. Qiu, H.B. Sun, Plasmonic-assisted graphene oxide artificial muscles, *Adv. Mater.*, 31 (2019) 1806386.
- [8] S. Ruiz, J.A. Tamayo, J.D. Ospina, D.P.N. Porras, M.E.V. Zapata, J.H.M. Hernandez, C.H. Valencia, F. Zuluaga, C.D.G. Tovar, Antimicrobial films based on nanocomposites of chitosan/poly(vinyl alcohol)/graphene oxide for biomedical applications, *Biomolecules*, 9 (2019) 109.
- [9] L.L. Ou, B. Song, H.M. Liang, J. Liu, X.L. Feng, B. Deng, T. Sun, L.Q. Shao, Toxicity of graphene-family nanoparticles: a general review of the origins and mechanisms, *Part. Fibre Toxicol.*, 13 (2016) 57.
- [10] Y. Volkov, J. McIntyre, A. Prina-Mello, Graphene toxicity as a double-edged sword of risks and exploitable opportunities: a critical analysis of the most recent trends and developments, *2D Mater.*, 4 (2017) 022001.
- [11] X.Y. Yuan, D. Peng, Q.Y. Jing, J.W. Niu, X. Cheng, Z.J. Feng, W. Wu, Green and effective removal of aqueous graphene oxide under UV-light irradiation, *Nanomaterials*, 8 (2018) 654.
- [12] T. Li, C.Z. Zhang, C.Y. Gu, Study on degrading graphene oxide in wastewater under different conditions for developing an efficient and economical degradation method, *Environ Technol.*, 38 (2017) 2999–3006.
- [13] Y. Zou, X. Wang, Y. Ai, Y. Liu, J. Li, Y. Ji, X. Wang, Coagulation behavior of graphene oxide on nanocrystalline Mg/Al layered double hydroxides: batch experimental and theoretical calculation study, *Environ. Sci. Technol.*, 50 (2016) 3658–3667.
- [14] J. Wang, X. Wang, L. Tan, Y. Chen, T. Hayat, J. Hu, A. Alsaedi, B. Ahmad, W. Guo, X. Wang, Performances and mechanisms of Mg/Al and Ca/Al layered double hydroxides for graphene oxide removal from aqueous solution, *Chem. Eng. J.*, 297 (2016) 106–115.
- [15] Y. Zou, X. Wang, Z. Chen, W. Yao, Y. Ai, Y. Liu, T. Hayat, A. Alsaedi, N.S. Alharbi, X. Wang, Superior coagulation of graphene oxides on nanoscale layered double hydroxides and layered double oxides, *Environ. Pollut.*, 219 (2016) 107–117.
- [16] J. Wang, Y. Li, W. Chen, J. Peng, J. Hu, Z. Chen, T. Wen, S. Lu, Y. Chen, T. Hayat, B. Ahmad, X. Wang, The rapid coagulation of graphene oxide on La-doped layered double hydroxides, *Chem. Eng. J.*, 309 (2017) 445–453.
- [17] L. Duan, R.J. Hao, Z. Xu, X.Z. He, A.S. Adeleye, Y. Li, Removal of graphene oxide nanomaterials from aqueous media via coagulation: effects of water chemistry and natural organic matter, *Chemosphere*, 168 (2017) 1051–1057.
- [18] X. Yuan, J. Niu, Y. Lv, Q. Jing, L. Li, Ultrahigh-capacity and fast-rate removal of graphene oxide by calcined MgAl layered double hydroxide, *Appl. Clay Sci.*, 156 (2018) 61–68.
- [19] X.Y. Yuan, J.W. Niu, J.J. Zeng, Q.Y. Jing, Cement-induced coagulation of aqueous graphene oxide with ultrahigh capacity and high rate behavior, *Nanomaterials*, 8 (2018) 574.
- [20] Z.X. Gan, X.L. Wu, M. Meng, X.B. Zhu, L. Yang, P.K. Chu, Photothermal contribution to enhanced photocatalytic performance of graphene-based nanocomposites, *ACS Nano*, 8 (2014) 9304–9310.
- [21] Y. Shen, Q.L. Fang, B.L. Chen, Environmental applications of three-dimensional graphene-based macrostructures: adsorption, transformation, and detection, *Environ. Sci. Technol.*, 49 (2015) 67–84.
- [22] Y.Y. Liu, W. Jin, Y.P. Zhao, G.S. Zhang, W. Zhang, Enhanced catalytic degradation of Methylene Blue by Alpha-Fe<sub>2</sub>O<sub>3</sub>/graphene oxide via heterogeneous photo-Fenton reactions, *Appl. Catal. B*, 206 (2017) 642–652.
- [23] N. Liu, W.Y. Huang, X.D. Zhang, L. Tang, L. Wang, Y.X. Wang, M.H. Wu, Ultrathin graphene oxide encapsulated in uniform MIL-88A(Fe) for enhanced visible light-driven photodegradation of RhB, *Appl. Catal. B*, 221 (2018) 119–128.
- [24] D. Robati, B. Mirza, M. Rajabi, O. Moradi, I. Tyagi, S. Agarwal, V.K. Gupta, Removal of hazardous dyes-BR 12 and Methyl Orange using graphene oxide as an adsorbent from aqueous phase, *Chem. Eng. J.*, 284 (2016) 687–697.
- [25] S.T. Yang, S. Chen, Y.L. Chang, A.N. Cao, Y.F. Liu, H.F. Wang, Removal of Methylene Blue from aqueous solution by graphene oxide, *J. Colloid Interface Sci.*, 359 (2011) 24–29.
- [26] K.P. Liu, H.M. Li, Y.M. Wang, X.J. Gou, Y.X. Duan, Adsorption and removal of Rhodamine B from aqueous solution by tannic

acid functionalized graphene, *Colloids Surf. A*, 477 (2015) 35–41.

- [27] A. Ghanadzadeh, A. Zeini, A. Kashef, M. Moghadam, Concentration effect on the absorption spectra of Oxazine1 and Methylene Blue in aqueous and alcoholic solutions, *J. Mol. Liq.*, 138 (2008) 100–106.

- [28] T. Szabó, E. Tombácz, E. Illés, I. Dékány, Enhanced acidity and pH-dependent surface charge characterization of successively oxidized graphite oxides, *Carbon*, 44 (2006) 537–545.

## Supplementary information

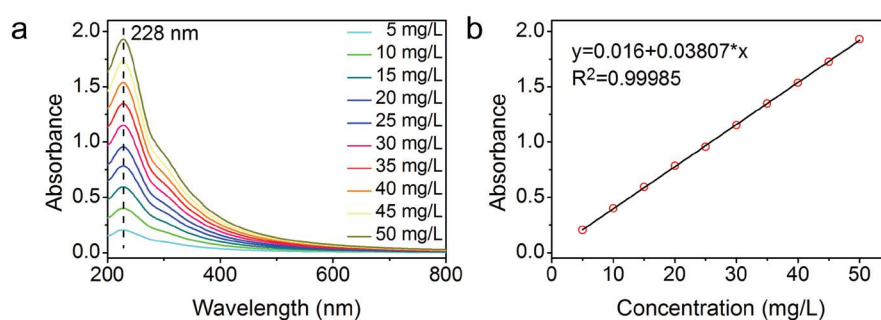


Fig. S1. (a) UV-Vis absorption spectra of GO suspension with different concentrations and (b) the correlation between GO concentrations and its UV absorbance intensity at 228 nm.

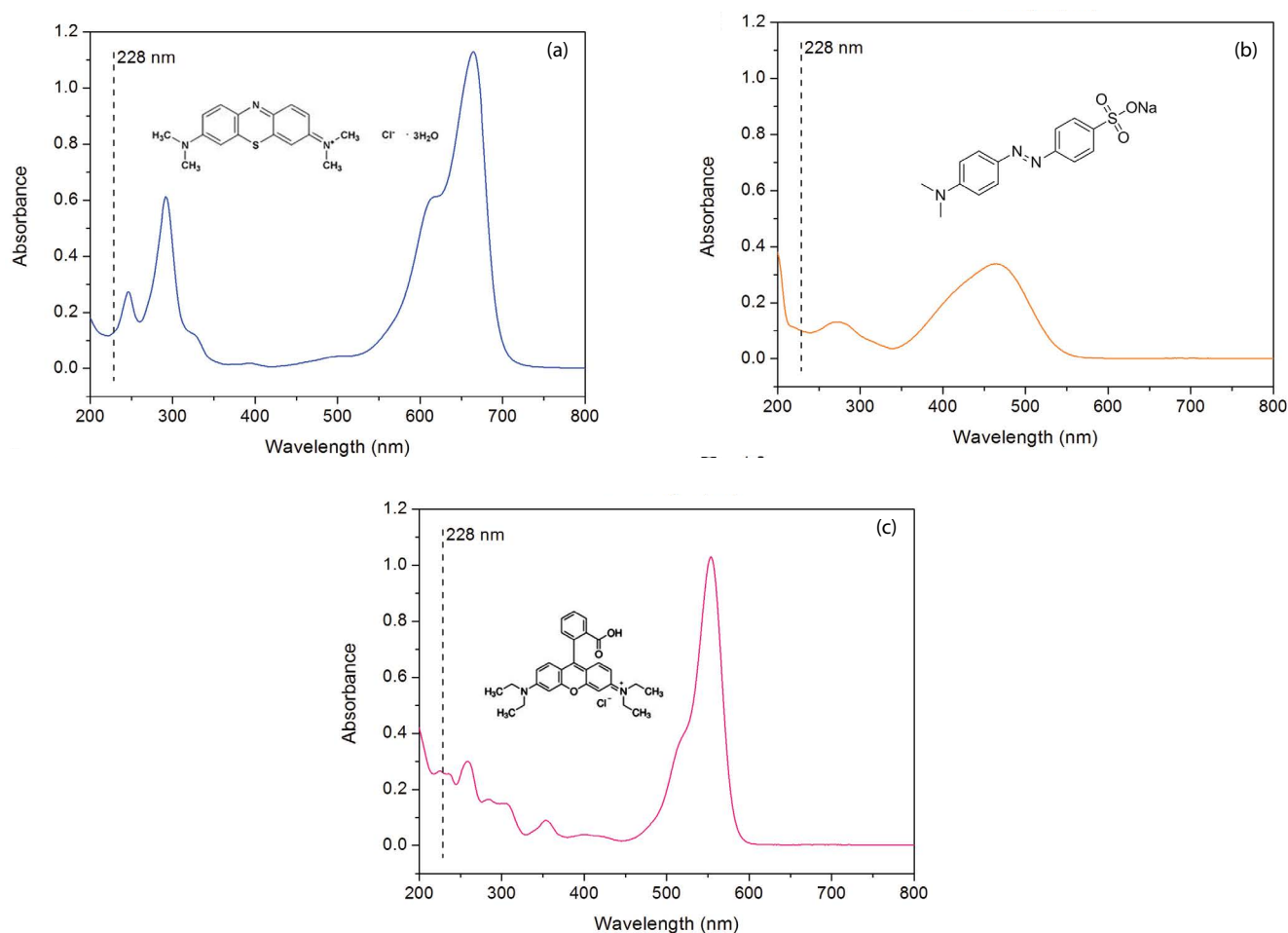


Fig. S2. UV-Vis absorption spectra of (a) MB, (b) MO and (c) RhB. The concentrations of the dyes are all 5 mg/L. Inset: structure of the dyes. They all have six-membered rings.

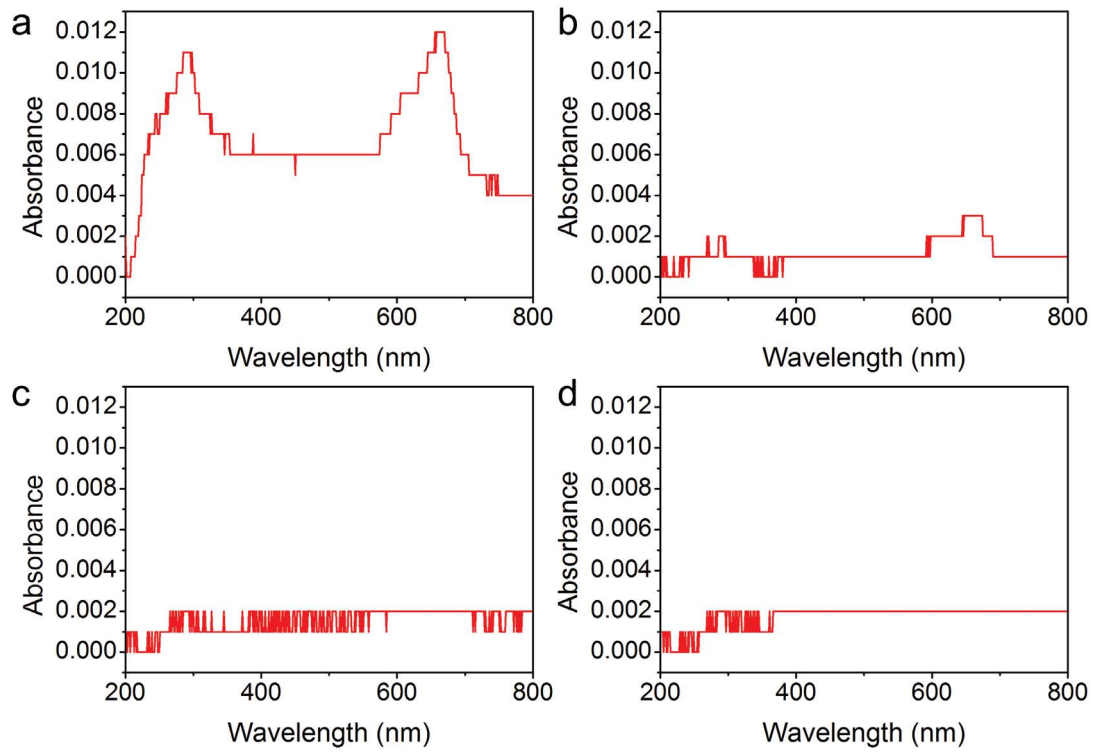


Fig. S3. UV-Vis spectra of MB aqueous solutions (5 mg/L) after adsorption in the presence of ACP. The amounts of ACP are (a) 50 mg/L, (b) 100 mg/L, (c) 200 mg/L, and (d) 400 mg/L.

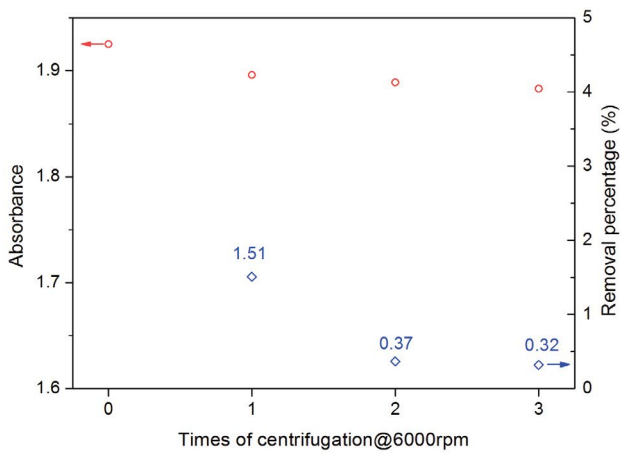


Fig. S4. Absorbance (red dot) and removal percentage (blue dot) of GO after centrifugation of different times. Speed of revolution is 6,000 rpm and the centrifugal time is 5 min.

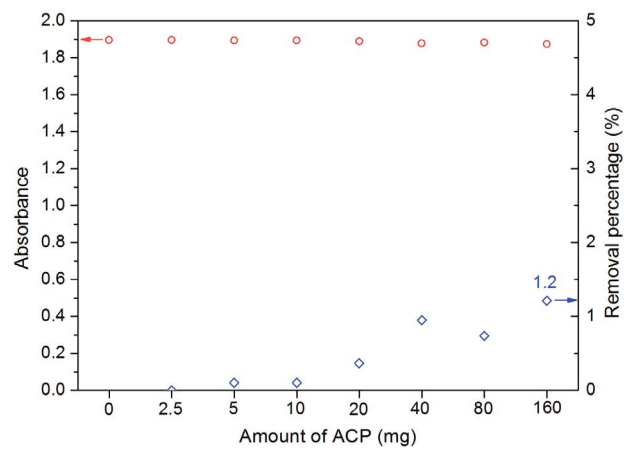


Fig. S5. Absorbance at 228 nm (red dot) and the removal percentage (blue dot) of 10 mL GO suspension (50 mg/L) after adsorption in the presence of ACP.

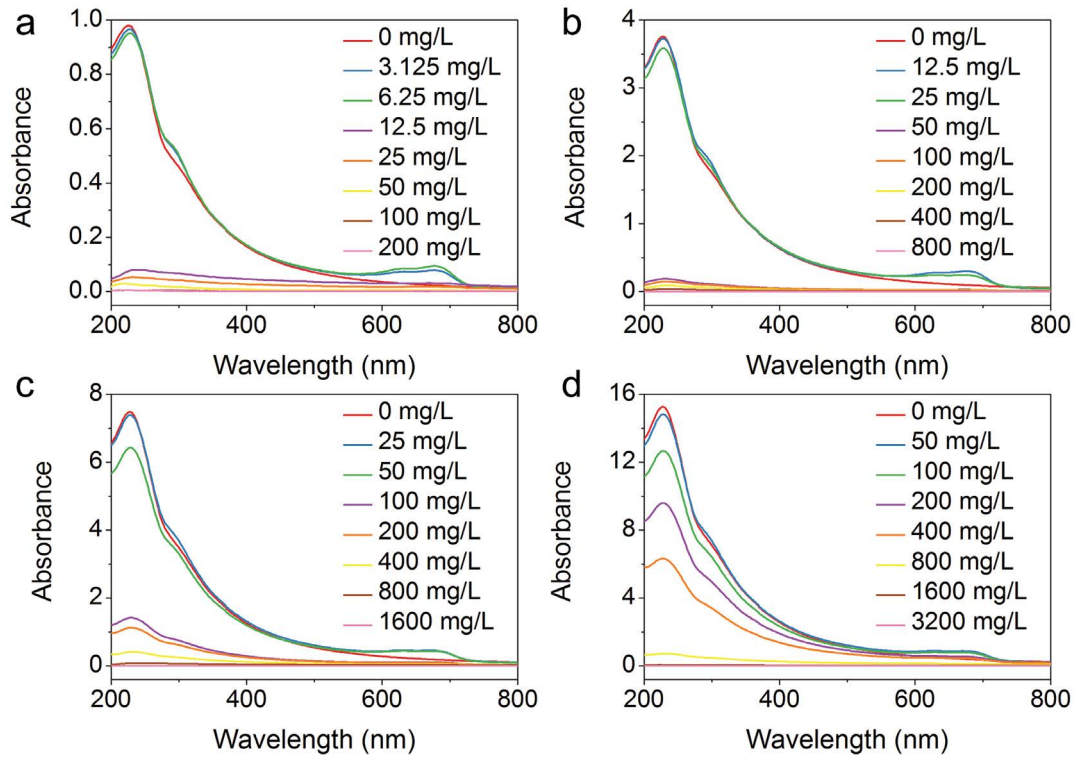


Fig. S6. Absorption spectra after the modified coagulation experiments. The initial GO concentration was about (a) 25, (b) 100, (c) 200, and (d) 400 mg/L.